A New Look at Calibration and Use of Eppley Precision Infrared Radiometers. Part II: Calibration and Use of the Woods Hole Oceanographic Institution Improved Meteorology Precision Infrared Radiometer*

RICHARD E. PAYNE AND STEVEN P. ANDERSON

Department of Physical Oceanography, Woods Hole Oceanographic Institution, Woods Hole, Massachusetts

(Manuscript received 16 January 1998, in final form 20 August 1998)

ABSTRACT

For some years, investigators have made measurements of downwelling longwave irradiance with the Eppley Precision Infrared Radiometer (PIR), recording the values of thermopile voltage and body and dome thermistor resistances and combining them in data processing. Part I of this paper reviews previous work on the processing equation and presents an improved equation. It establishes that the standard single-output Eppley has an inherent uncertainty of 5%. By measuring the three possible outputs separately and comparing them in the improved equation, the inherent accuracy can be improved to 1.5%. Part II presents a method of calibrating the Eppley PIR for the three-output equation using an easily constructed blackbody cavity in a temperature bath capable of a 0°–50°C temperature range. Calibration of PIR thermistors is recommended since occasionally one is found out of specifications.

An outdoor comparison of 15 PIRs calibrated with the technique was carried out in groups of four, with one PIR used in all of the groups as a standard of comparison. The mean differences and 1-min standard deviations between 12 individual PIRs and this standard over comparison periods of 10–22 days were less than 6.0 and 11 W m^{-2}, respectively. Only two of the PIRs and a standard single-output Eppley PIR (calibrated by Eppley) had mean differences and standard deviations greater than 7 and 11 W m^{-2}, respectively. Although the new calibration procedure yielded consistent results in the mean, at times the longwave measurements diverged by up to 45 W m^{-2} for several hours. Some of these events are attributable to confirmed pinholes in the dome filter, but others are left unexplained.

1. Introduction

Accurate measurements of the net surface heat flux are essential for improving our understanding of the interaction and coupling between the atmosphere and the ocean. Of the components of the net surface heat flux, the longwave radiation is historically the least observed and has been difficult to measure accurately at sea. As a result, many air–sea interaction studies have relied on climatology or parameterizations based on sparse data to estimate net longwave radiation.

The sensor used widely for these marine measurements is the Eppley Precision Infrared Radiometer (PIR). Fairall et al. (1998, hereafter referred to as Part I) review the theory of operation of the Eppley PIR and discuss the accuracy and calibration of the two commonly used forms of the Eppley PIR. The two forms differ only slightly. The single-output PIR employs a battery-powered circuit to compensate for the body temperature, while the three-output PIR allows the user to record body and dome thermistor temperatures and thermopile voltage separately. Part I presents a revised temperature compensation equation for the three-output PIR. Although Part I reports on data collected with these instruments at sea, the Eppley PIR is not designed to withstand the corrosive and destructive forces found in the marine environment for an extended period of time.

The Upper Ocean Processes Group at the Woods Hole Oceanographic Institution (WHOI) has deployed the Eppley PIR to measure downwelling longwave radiation from moored buoys at various midocean locations for more than 10 years (Weller et al. 1990; Weller and Anderson 1996). There have been both successes and failures along the way. The experiences obtained while deploying these PIRs have led to the modification of the stock Eppley PIR for use in the marine environment as well as to the improvement of the calibration techniques.

The result is the Improved Meteorology (IMET) PIR, which is designed for use on buoy- and ship-mounted meteorological systems. These advances show promise

* Woods Hole Oceanographic Institution Contribution Number 9723.

Corresponding author address: Dr. Richard E. Payne, Department of Physical Oceanography, Woods Hole Oceanographic Institution, Woods Hole, MA 02543.

FIG. 1. Photograph of Eppley (right) and IMET (left) PIRs.

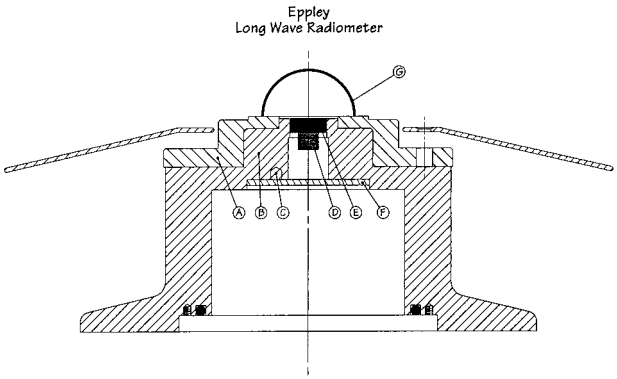

FIG. 2. Cross-section sketch of the Eppley PIR. Significant parts are (a) top and dome mount (stainless steel), (b) pyrgeometer body (cast bronze), (c) hole in which body thermistor is potted, (d) thermopile, (e) thermopile cap containing flat black-coated flux-sensitive surface, (f) internal radiation shield (aluminum), and (g) silicon dome.

of making the measurement of downwelling longwave radiation a routine operation at sea. Section 2 of this paper describes how the stock Eppley PIR was modified for the IMET PIR. The IMET PIR calibration facility and procedure are described in section 3. Section 4 reports on the intercomparison of 15 individual IMET PIR sensors, and section 5 contains the summary and conclusions.

2. The IMET PIR

Drummond et al. (1970) describe an instrument for measuring incident longwave radiation on a routine basis. This instrument used a thermopile and a dome filter that allowed a portion of the infrared radiation to pass, but excluded shortwave radiation. With substantial modifications, this became the Eppley PIR, which was manufactured and sold starting in 1972. The PIR design was slightly modified in 1976, when the dome material was changed to silicon and a thermistor glued to the dome interior was added. The instrument has remained essentially unchanged since then.

Figure 1 is a photograph of the Eppley and IMET PIRs. A cross section of the Eppley PIR appears in Fig. 2. Longwave radiation is incident through the silicon hemisphere. This dome is held by a stainless steel collar that covers the top of the instrument. The rest of the sensor body is made of cast bronze. A thin white-painted aluminum disk provides shielding from shortwave radiation for the body and dome mounting. Beneath the dome is a disk coated with a flat black lacquer mounted on the base of an inverted T-shaped piece of aluminum. A thermopile is wound on the T, and the arms of it are fixed to the sensor case with screws (Fig. 3), providing thermal contact with the case. The thermopile measures the temperature between the black surface and the instrument case. Two thermistors are potted into the sensor case near the points of attachment of the T. Another thermistor is cemented to the inside of the dome at its base. A schematic of the Eppley PIR circuitry is shown in Fig. 4. This circuitry provides a compensation for the body temperature, resulting in a single-output voltage approximately proportional to the total longwave irradiance incident on the PIR. Note that the dome thermistor is not used in the battery compensation circuit.

A multilayer dielectric coating on the inside of the dome in combination with the silicon material forms a filter. According to Eppley Laboratory, Inc. (1976), the

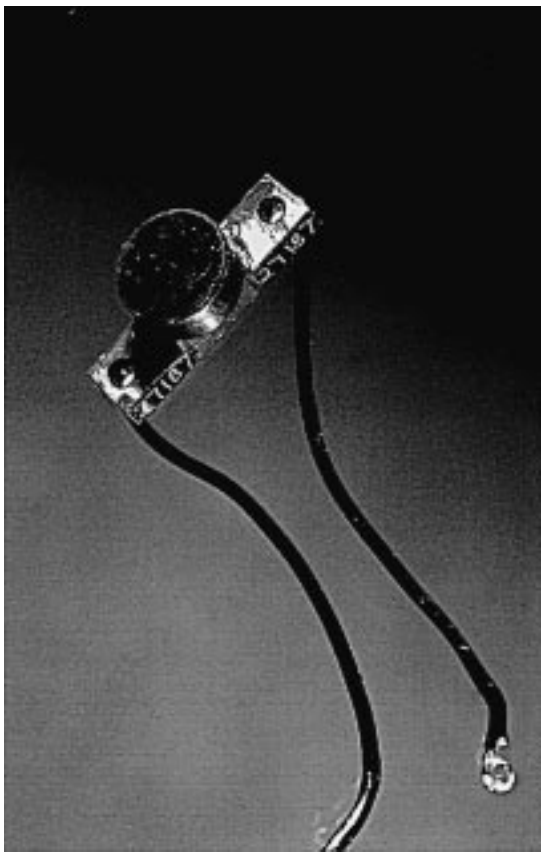

FIG. 3. Photograph of thermopile assembly showing mounting holes and cap.

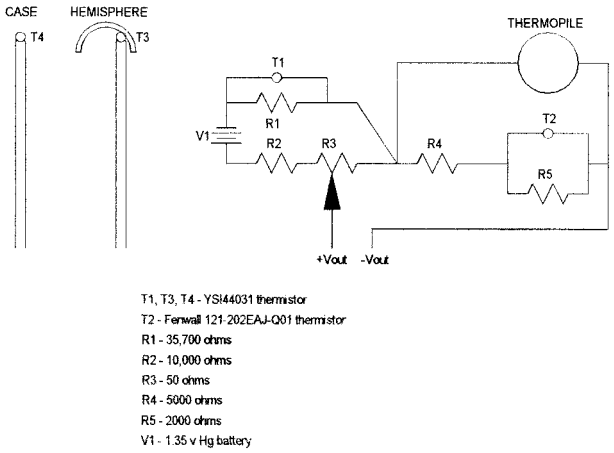

FIG. 4. Eppley PIR circuitry: V_{out} is single voltage of standard Epply model; T_1 and T are thermistors potted in case and are equivalent; T_2 provides compensation for the thermopile temperature coefficient; and T_3 is cemented to the inside of the dome.

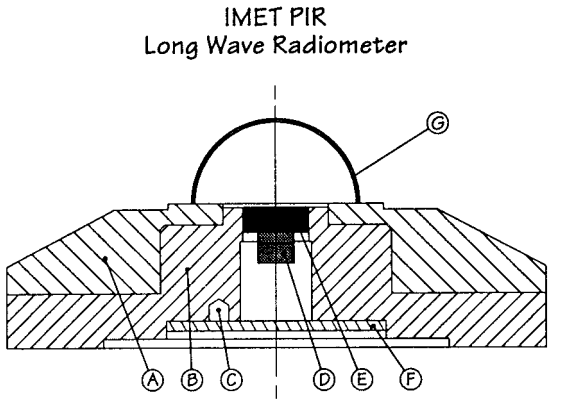

FIG. 5. Cross-section sketch of IMET PIR. Significant parts and materials are (a) radiation shield and mount (white-painted aluminum), (b) body (aluminum), (c) hole into which body thermistor is potted, (d) thermopile, (e) thermopile cap containing flat black-coated flux-sensitive surface, (f) internal radiation shield, and (g) silicon dome.

filter has a transmission coefficient of approximately 0.5 in the range from 4 to 50 μm with a sudden onset of transmission between 3 and 4 μm that slowly decreases at long wavelengths to 0.3–0.4, approaching 50 μm. The detailed characteristics of individual filters vary somewhat (G. Kirk 1995, personal communication). The flat black paint coating the disk is made to Eppley's specifications and is virtually identical to Parson's black lacquer (G. Kirk 1995, personal communication). Tests of Parson's black lacquer at the National Physical Laboratory, London, England, with lamps at color temperatures of 200°, 1000°, and 2580°C, yielded absorption factors of 0.985, 0.980, and 0.985, respectively, indicating an absorption factor close to 0.985 over a wide range of wavelengths (Eppley information sheet: Eppley–Parsons optical black lacquer). Albrecht and Cox (1977) state that the spectral response is uniform from 3 to 50 mm.

In its standard configuration, the Eppley PIR is adapted poorly to ocean buoy deployments. The variety of metals used in the stock Eppley PIR include bronze, aluminum, and stainless steel, which, when exposed to saltwater, assures galvanic corrosion. In addition, the radiation shield is somewhat fragile and can catch lines used in buoy deployment and recovery. After discussing the design of the PIR with Eppley personnel, we modified the sensor design to better suit our application. The IMET PIR is available from Eppley Laboratory, Inc. on special order.

The modified PIR design is shown in Figs. 1 and 5. The radiation shield has been eliminated. The dome collar and the body are both machined aluminum painted with Ameron Siloxane PSX 700, a rugged, two-part, bright white paint containing both epoxy and acrylic polyurethane. Since all mounting screws are within O-rings, there is no place for galvanic corrosion to occur. The IMET design has other advantages. Foot (1986) found evidence that there were temperature gradients within the Eppley PIR that caused significant errors. Since aluminum has a higher heat conductivity than either stainless steel or bronze, temperature gradients within the IMET sensor are minimized. In addition, the sensor is designed to be an endcap to a tube-holding analog and digital circuitry, thus minimizing the cable length from the sensor and facilitating mounting on a buoy.

The behavior of either the Eppley or IMET design of the PIR is represented by (11) in Part I. Repeated here, the incident longwave radiation H is determined by

$$H = \underset{1}{\sigma T_s^4} + \underset{2}{A\Delta T} + \underset{3}{B\sigma(T_s^4 - T_d^4)}, \tag{1}$$

where ΔT is the temperature difference across the thermopile, σ is the Stefan–Boltzmann constant, T_s is the temperature of the blackened upper surface of the thermopile, T_d is the dome temperature, and A and B are constants of calibration. The thermopile surface temperature T_s is the sum of the body temperature, T_c, and ΔT. The thermopile relationship is

$$\Delta T = \alpha \Delta V, \tag{2}$$

where ΔV is the voltage across the thermopile and α is the thermopile constant. The Eppley thermopile has a Seebeck coefficient of 40 (μV °C^{-1})/junction, 60 junctions, and an efficiency of 60% at 20°C (J. Hickey 1993, personal communication). This yields a value of α of 694 °C V^{-1} at 20°C. The temperature dependence of the thermopile calibration can be ignored since it is small and largely compensated by the passive thermistor circuit in parallel with it. Constants A and B are to be determined by calibration, and neither A nor B is dependent on temperature.

3. Calibration

a. Calibration background

Although Eppley provides a calibration service for its single-output PIR, such a service is not available in the United States for the three-output version. Therefore, in order to encourage wider use of the three-output version, we describe in some detail the calibration method we use. With the exception of the blackbody cavity, it employs equipment readily available in any laboratory prepared to make accurate temperature calibrations. We describe the design of the blackbody cavity in sufficient detail for duplication.

Our calibration method of the three-output PIR was derived from the pioneering work of Albrecht and Cox (1977), who used a conical blackbody with large thermal mass. The key to this procedure lies in finding a point at which T_s and T_d are equal. At this point, the dome term drops out of (1), and the calibration constant A can be estimated directly. Starting with the cavity at a low temperature (−10°C), Albrecht and Cox insert the PIR and record its outputs while the cavity temperature drifts slowly upward. Since the dome and thermopile have different thermal time constants (we estimate from our results that the time constants are roughly 12 and 4 s respectively), the T_d and T_s curves cross and A can be evaluated at that point. Albrecht and Cox (1977) then use this value of A to make a least squares fit of $H - \sigma T_s^4 - A\Delta T$ versus $\sigma(T_s^4 - T_d^4)$ to get B.

Brogniez et al. (1986) have a different technique. The pyrgeometer was faced into a conical blackbody cavity, and a stream of temperature-controlled air was blown across the dome. With this arrangement, the temperature of the dome can be varied slowly and independently. Plotting values of $\sigma(T_c^4 - T_s^4)/\Delta V$ versus $\sigma(T_s^4 - T_d^4)/\Delta V$ yields a straight line, of which the slope is B and the y intercept is A.

A third calibration technique is that of Philipona et al. (1995), who use a version of the pyrgeometer equation with expanded T_s:

$$H = \frac{1 + k_1\sigma T_c^3}{C}\Delta V + k_2\sigma T_c^4 - k_3\sigma(T_d^4 - T_c^4). \quad (3)$$

Philipona et al. (1995) point the pyrgeometer into a cylindrical blackbody cavity and control the body and dome temperature, T_d and T_c, as well as the temperature of the cavity. By varying the temperatures separately, Philipona et al. can determine the k_i and C individually. They find that k_2 is 1.00 within about 0.05% for the five PIRs they tested, agreeing well with the derivation of Part I. Although Philipona et al.'s constants yield the fundamental constants of the dome, they cannot be converted readily into our calibration constants.

b. Thermistor calibration

Eppley uses YSI-type 44031 glass encapsulated, 0.2°C interchangeable thermistors in the construction of the PIR. Our 20 years of experience in thermistor calibrations for current meters leads us to be skeptical of all thermistors, especially when they are used over periods of years (Payne et al. 1976). Although we calibrate the thermistors in our PIRs at intervals of approximately 1 year, these calibrations do not extend over a long enough period to make any statements about possible drift rates. We have observed, however, that the dome thermistors in 6 of the 223 PIRs we calibrated thus far differed from the manufacturer's nominal curve by 0.1°–0.4°C.

To calibrate the PIR thermistors, a small aluminum can, constructed for this purpose, is attached to the back of the PIR (IMET PIR only). The can keeps the PIR watertight but gives good thermal contact with water. The whole case is then immersed into a Hart calibration bath whose temperature is controlled to within 2 mK. The bath temperature is measured with a platinum resistance thermometer to an accuracy of 5 mK. Resistance of both thermistors is measured at 5°C intervals from 0° to 35°C, and the results are fitted to the Steinhart–Hart (Steinhart and Hart 1968) equation. Temperatures computed from thermistor resistances are then accurate to about 10 mK. Sufficient time is allowed at each temperature so that gradients within the PIR have disappeared, but gradients certainly exist under field and longwave calibration conditions. The thermistor temperatures thus represent either body or dome temperature less accurately under operational (or field) conditions. The inaccuracies introduced by thermal gradients within the PIR body and dome can be greater than 0.2°C (Philipona et al. 1995).

Although Eppley uses 0.2°C interchangeable-grade thermistors, our calibration results show that not all thermistors fall within these limits. Figure 6 shows a histogram of differences between the calibrated sensor curve and the manufacturer's curve in millidegrees kelvin evaluated at 15°C. Thus, the temperature differences are between the manufacturer's standard curve and the actual thermistor curve at a given value of thermistor resistance. All of the body thermistors fall within the 0.2°C limits, but several of the dome thermistors do not. A 0.2°C bias in body temperature is equivalent to a 1.2 W m^{-2} bias in total longwave flux through term 1 in Eq. (1). The same bias in the dome temperature can lead to a bias of order 0.1 W m^{-2} in total flux. It is fortunate that the longwave flux is fairly insensitive to the accuracy of the dome temperature measurement.

c. Blackbody cavity

A source of known longwave radiation is a fundamental requirement. We have constructed a blackbody cavity (BBC) to provide this. A cross-sectional sketch of the BBC is shown in Fig. 7. It is constructed of 0.020-in.-thick copper sheet with three brass rings providing stiffening. The bottom forms a cone with an angle of approximately 70° to prevent radiation that enters the

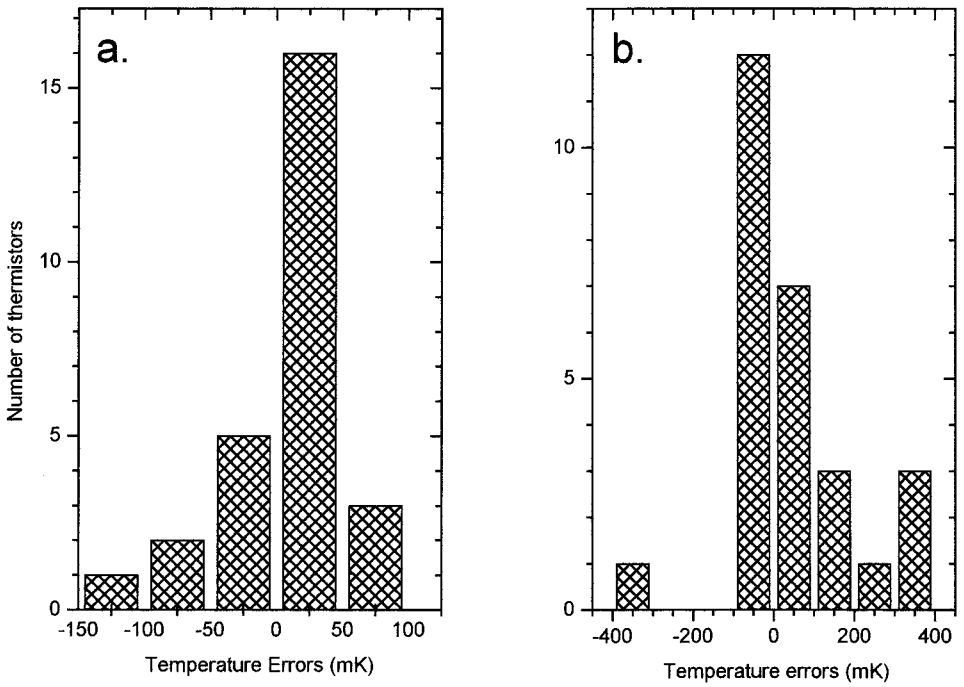

FIG. 6. Histograms of thermistor differences, calibration curves minus manufacturer's nominal curve: (a) body thermistors and (b) dome thermistors.

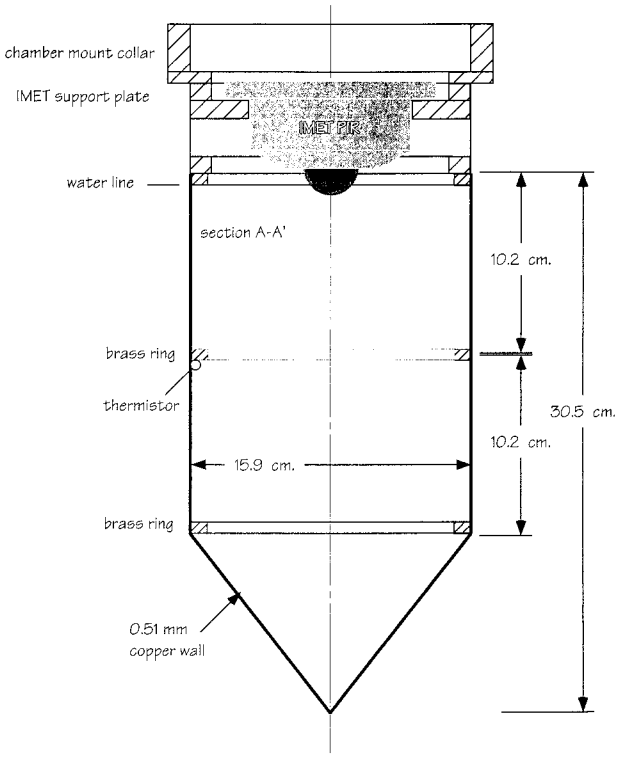

FIG. 7. Cross section of blackbody cavity.

aperture from being reflected back to the aperture. An aluminum plate, 3.2 mm thick and with a hole a little larger than the base diameter of the dome, terminates the top end of the cylinder. The PIR is suspended so that its body is less than 1.5 mm above the plate, with the dome protruding through the hole. The entire inside of the BBC is painted with Eppley's version of Parson's black lacquer to improve its effective emissivity. In use, the BBC is immersed to the level of the aluminum plate at the top end in a mechanically stirred calibration water bath whose temperature can be varied from 0° to 50°C and is constant to within 10 mK through each calibration run. A single thermistor measures the temperature on the inside to compare with the bathwater temperature and is mounted under one of the brass rings so as not to be radiated on directly by a PIR that is being calibrated. The water temperature is measured with the platinum resistance thermometer to an accuracy of 5 mK. The BBC is assumed to be at the thermistor temperature, but the bath temperature is monitored as a check. Submersing the BBC in the bath means that we have an effectively infinite heat sink whose ability to absorb heat from the BBC is limited only by the heat conductivity of the 0.020-in.-thick copper walls.

Sparrow et al. (1962) describe the results of computations to determine the emissivity of cylindrical blackbody cavities at wall emissivities of 0.5, 0.75, and 0.9 and at length-to-diameter ratios of 0.25 to 4. Interpolating and extrapolating from Sparrow et al.'s tables for our value of length/diameter of 1.25 and wall emissivity of 0.985, we estimate the effective emissivity at

the center of the aperture to be 0.995. Applying the results of Sparrow et al., our cylinder probably has an uncertainty of at least 0.005. For computation of the PIR constants, we assume that the effective emissivity of the BBC is 1.000. Sparrow et al. also provide estimates of the variation of effective emissivity across the aperture. With the dimensions of our cylinder and aperture, the variation of the apparent emissivity across the aperture is no more than 0.001. Note that caution must be used to ensure that no condensation occurs inside the cavity, since that could change the emissivity appreciably.

We plan to build a new BBC with increased L/d ratio so that we can increase the effective emissivity to be indistinguishable from 1.000. Decreasing the diameter to 7.5 cm and increasing the length to 2.3 cm with a 60° cone on the bottom will increase L/d to at least 3, yielding an apparent emissivity of 0.997 for a wall emissivity of 0.9. Painting the walls with Parson's black lacquer will then increase the effective emissivity to immeasurably less than 1.000.

d. Longwave calibration procedure

We have followed the Albrecht and Cox (1977) technique in developing our calibration procedure. Since it is impractical to vary the BBC temperature over a substantial range relative to the absolute temperature, A and B must be determined using a limited temperature range. The idea is to determine A from a set of conditions in which T_s and T_d are equal so that the B term disappears. After A is resolved, B is determined in conditions in which both terms contribute to the measurement. Like Albrecht and Cox (1977), we take advantage of the fact that the thermopile has a shorter time constant than the dome, and in turn, the dome has a shorter time constant than the body. Our general procedure is to face the PIR into a source that is at a substantially different temperature from the BBC for a short time, thus preconditioning the dome temperature. Then, we quickly move the PIR to the BBC and record the thermopile and temperature outputs.

As an illustration, the time series of PIR temperature outputs for a single calibration run are presented in Fig. 8. The data are recorded at 1 Hz with a Keithley Model 2000 Digitial Multimeter with internal scanner. The resistance measurements have an accuracy of 2 ohms in the range of calibration temperatures. For the YSI-type 44031 thermistors used in the PIR, this is equivalent to about 4 mK.

The steps to the procedure are as follows. 1) The PIR outputs are recorded for 1 min with the PIR at room temperature to assure temperature stability. 2) The PIR is inverted over water at 50°C for 1 min to precondition the dome temperature. Note the rapid warming of T_s and the less rapid response of T_d. 3) The PIR is moved into the BBC, and T_s cools rapidly. 4) As the dome cools off over the cold BBC, the T_d eventually crosses over the T_s record. The time series is interpolated to the crossover point $T_s = T_d$ using several points on either side of this point, and A is determined using the known BBC temperature, T_s and T_c. 5) Approximately 5 min after the PIR is inserted into the BBC, the rate of change in T_s, T_d, and T_c is nearly equal. Then B is determined using the BBC temperature, T_s, T_c, and T_d combined with the A constant determined earlier in the record. Note that the BBC varies by only 15 mK during the calibration run.

The procedure is repeated for a specified six sets of conditions that give a sufficient range of BBC temperatures—which are realizable in our laboratory—to yield valid values of the constants A and B (Table 1). For BBC temperatures above 10°C, the preconditioning is conducted over ice, but otherwise, the procedure is the same. An example calibration run with cold preconditioning is shown in Fig. 9.

After converting the raw data to temperatures and temperature differences, four records centered on the two records either side of $T_s^4 - T_d^4 = 0$ and the last record in the file are extracted from the file for each run and concatenated into a single file. A set of linear interpolations gives the value of each of the variables at $T_s^4 - T_d^4 = 0$. The slope of a line least squares fitted to the values of $\sigma(T_c^4 - T_s^4)$ versus $(T_s - T_c)$ is B. Constant A is computed as the slope of a line least squares fitted to the values of $\sigma(T_c^4 - T_s^4) - B(T_s - T_c)$ versus $\sigma(T_s^4 - T_d^4)$. The standard deviation between the radiation computed from the chamber temperatures and those computed from the last record with the derived constants is 2 W m^{-2} or less in the calibrations done thus far. Appendix A lists the calibrations performed from November 1994 through May 1998. The techniques were gradually improved from 1994 on, culminating with the introduction of the Keithley 2000 in April 1996.

From the appendix, it is apparent that 22 of the PIRs represented are quite uniform: A varies about 10% and B about 50% about their median values for all PIRs but one. PIR 27957 appears to be anomalous, although there is nothing obviously different about it when its parts are examined closely. For individual PIRs, the values cluster more closely with the standard deviation about the mean no more than 6.3% in A and 34% in B. Since there are no obvious drifts with time in either A or B for any of the PIRs, we will assume that the variations are due to uncertainties in the calibrations.

The effects of calibration uncertainties on total longwave heat flux computed from (1) depends on the relative values of the three terms. In summer conditions on our coast, typical values of the total longwave are 400 W m^{-2}, with term 1 contributing 400–450 W m^{-2} (night to day), the A term 0 to -80 W m^{-2}, and the B term 0 to -10 W m^{-2}. Equation (1) could be written as a function of the quantities derived exponentially:

$$H = H(T_c, \Delta T, T_D, A, B).$$

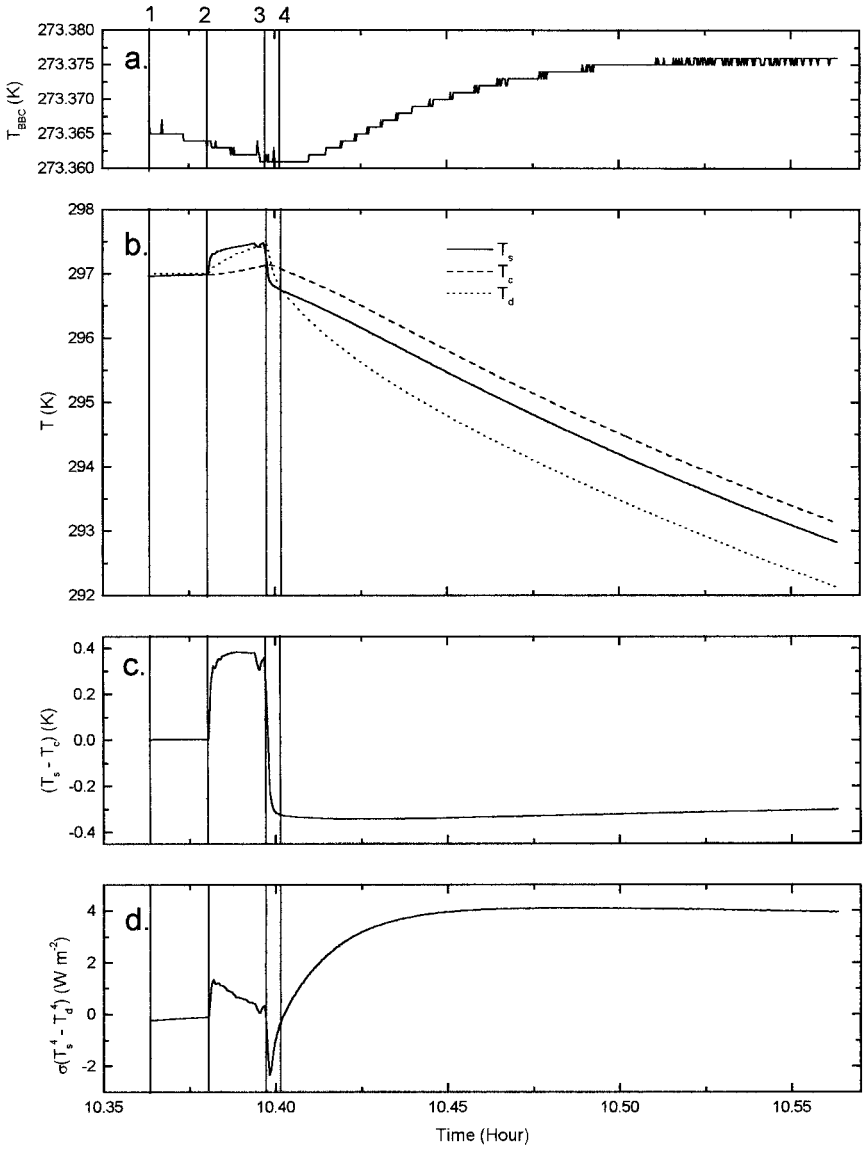

FIG. 8. Data from a hot-to-cold calibration run: (a) is the wall temperature of the BBC; (b) shows the PIR thermopile surface, body, and dome temperatures; and (c) is the temperature difference across the thermopile; (d) is the last term from (1). The numbered times are, respectively, the time at which the recording starts, the PIR is suspended over hot water, the PIR is placed in the BBC, and the Eq. (1) term 3 passes through zero.

TABLE 1. Calibration conditions.

Run	Precondition (°C)	BBC (°C)
A	50	0.1
B	50	5
C	50	10
D	Ice	30
E	Ice	40
F	Ice	50

The uncertainty in H due to errors in the parameters can be expressed as

$$\Delta H = \frac{\partial H}{\partial T_c}\Delta T_c + \frac{\partial H}{\partial \Delta T}\Delta(\Delta t) + \frac{\partial H}{\partial T_D}\Delta T_D + \frac{\partial H}{\partial A}\Delta A + \frac{\partial H}{\partial B}\Delta B, \quad (4)$$

which can be evaluated from (1). If the parameters are independent, then the total error in H is the square root of the sum of the squares of the individual terms in (4). Table 2 contains a set of parameter and error values as

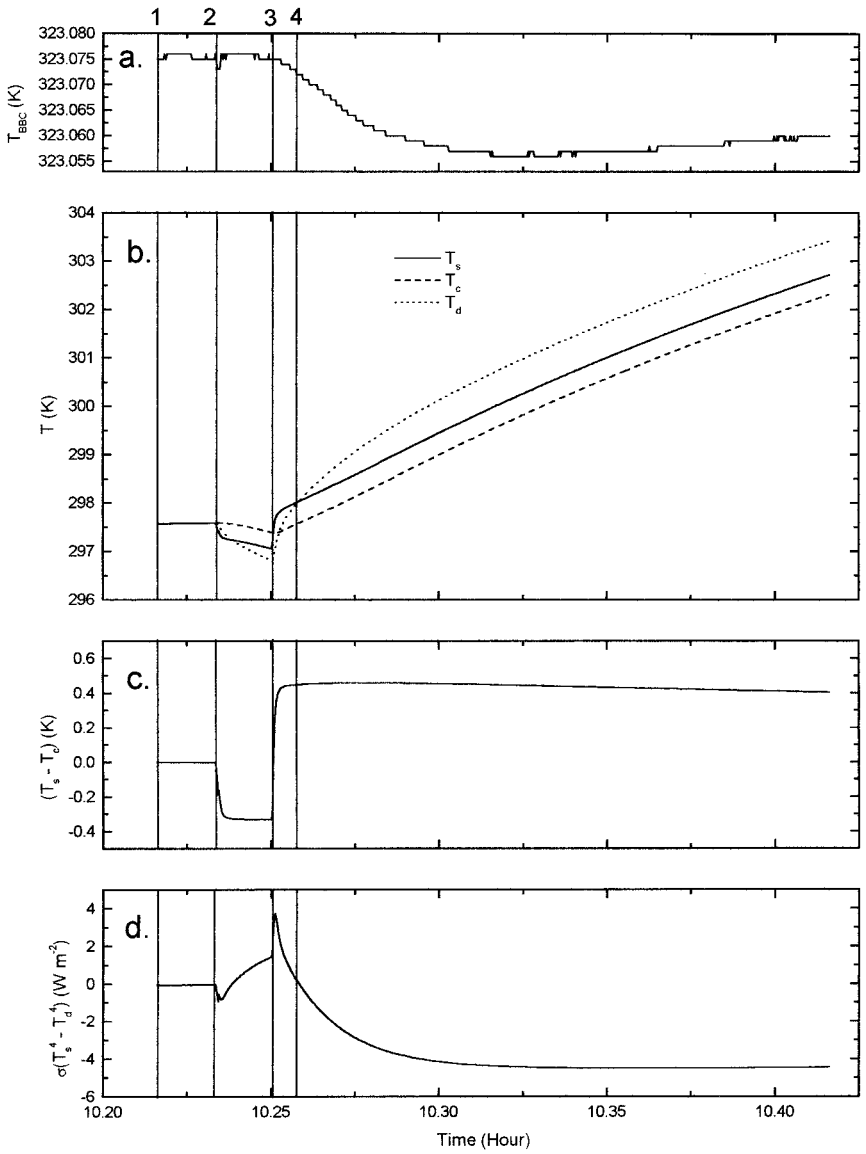

FIG. 9. Data from a cold-to-hot calibration run. Details are the same as for Fig. 8.

well as the total error in H to which they lead. The total uncertainty of 5.7 W m^{-2} is similar to the result derived in Part I and compares favorably with the values computed in Part I for the single-output Eppley PIR, 20 W m^{-2}.

TABLE 2. Summary of errors in longwave measurements.

Parameter	Value	Error	ΔH contribution
T_c	300 K	±0.1 K	±2.3 W m^{-2}
Δt	−0.2 K	±0.005 K	±2.7
T_D	301 K	±0.2 K	±2.6
A	390 W m^{-2} K^{-1}	4%	±3.1
B	2.8	4%	±0.8
		Total uncertainty in H	±5.7 W m^{-2}

4. PIR comparisons

In June, July, and August 1996, 15 IMET PIRs and 1 standard Eppley PIR were compared on the roof of a WHOI building in groups of four for periods of 10–22 days per group. The deployment site has an unobstructed view of the sky on a hill overlooking Nantucket Sound. Summer in Woods Hole, Massachusetts, is generally marked by frequent and rapid changes in weather conditions. During summer 1996, the surrounding waters were cooler than average, while there were frequent flows of moist air into the area, resulting in many foggy nights. However, cloudiness was less than an average summer, resulting in large values of the $T_s^4 - T_d^4$ term during the day.

A Campbell Scientific Model CR7 data logger was

TABLE 3. Summary of PIR comparisons.

PIR number	Length days	Mean LW	Min LW	Max LW	Group mean difference	Mean 28382 difference	rms difference	Comments
IMET 28382	21.9	380.3	308.3	426.3	2.7			
Eppley 26982	21.9	373.2	291.0	437.0	−4.4	−7.0	12.0	
IMET 27927	21.9	381.1	300.9	453.3	3.5	0.8	8.2	Shortwave leak
IMET 28463	21.9	375.8	306.5	421.4	−1.8	−4.5	5.6	
IMET 28382	10.4	383.7	317.0	427.9	−0.5			
IMET 27928	10.4	382.3	311.6	428.9	−1.9	−1.4	3.0	
IMET 28458	10.4	386.8	315.7	436.7	2.6	3.1	9.5	Shortwave leak
IMET 28460	10.4	384.1	311.2	430.9	−0.1	0.5	4.8	Shortwave leak
IMET 28382	13.1	382.1	317.2	430.6	4.9			
IMET 27026	13.1	372.6	304.1	424.6	−4.6	−9.5	11.1	
IMET 27363	13.1	376.4	309.2	426.6	−0.8	−5.7	5.2	
IMET 28381	13.1	377.6	312.0	426.3	0.4	−4.5	6.4	
IMET 28382	10.3	387.0	332.2	466.8	0.6			
IMET 27954	10.3	377.9	321.7	415.3	−8.5	−9.1	12.1	
IMET 27957	10.3	389.5	343.7	421.7	3.1	2.5	10.7	
IMET 28459	10.3	391.1	338.4	457.9	4.7	4.1	8.1	
IMET 28382	15.9	377.3	318.5	427.6	2.3			
IMET 27238	15.9	373.4	309.7	432.2	−1.6	−3.9	5.9	
IMET 28461	15.9	374.3	312.9	428.3	−0.7	−3.1	5.7	
IMET 28908	15.9	375.0	315.4	426.1	0.0	−2.3	4.4	

used to record 5-min averages of 1-s samples from the PIRs, an Eppley Precision Spectral Pyranometer (PSP) pyranometer, and an anemometer. The PSP output and the PIR thermopile voltage were measured directly. Each thermistor was connected in series to a 0.01%, 10 000-ohm Vishay resistor and the pair excited with a precise voltage from the CR7. The resulting voltage across the thermistor was recorded by the CR7.

One IMET PIR, serial number 28382F3, was selected arbitrarily out of the first group and deployed in all groups to give a basis of overall comparison. Each of the time periods had at least two virtually cloudless days and several foggy nights. This is significant because on foggy nights the contribution to total longwave flux from the thermopile and dome terms is close to zero, while on sunny days both terms are likely to have maximum values.

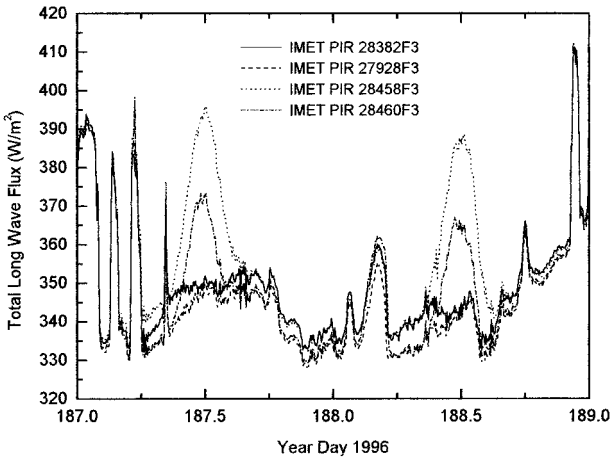

FIG. 10. Examples of shortwave leakage by domes. Note peaks in output of PIRs 28458F3 and 28460F3 during times of high shortwave irradiance. The abscissa is local time.

Before deploying the Eppley stock PIR 26982F3, we installed a fresh battery and adjusted the internal potentiometer following Eppley procedure (Eppley Laboratory, Inc., 1994). All PIRs and the PSP were leveled to within 0.1° of the vertical. The IMET PIRs have no external indication of the position of the dome thermistor. Since we have no way of controlling their azimuth on ship or buoy, we did not try to orient them azimuthally on the roof.

A statistical summary of the comparison appears in Table 3. The table is grouped by sets of four PIRs that were recorded together. In addition to the PIR serial numbers, the table includes the length of the data records in day; the mean, minimum, and maximum flux values recorded for each PIR; the mean difference of each PIR from the group mean; and the mean difference and root-mean-square difference of each PIR from serial number 28382F3.

Some of the PIRs show distinct evidence of leakage of shortwave radiation through the domes; three (noted in Table 3) are particularly serious. Figure 10 shows a detail from data from the second group for two consecutive clear days. Although all four pyrgeometers agree quite well through substantial nighttime fluctuations in longwave flux, IMET PIRs 28458F3 and 28460F3 have anomalous peaks during the day that are completely in phase with the shortwave irradiance. IMET PIR 27927F3 in the first group shows similar peaks. Early versions of the dielectric coating occasionally suffered from pinholes (J. Hickey 1993, personal communication), but Eppley thinks this problem was solved some years ago. Eppley found a pinhole in the dome coating of serial number 28458F3 and replaced

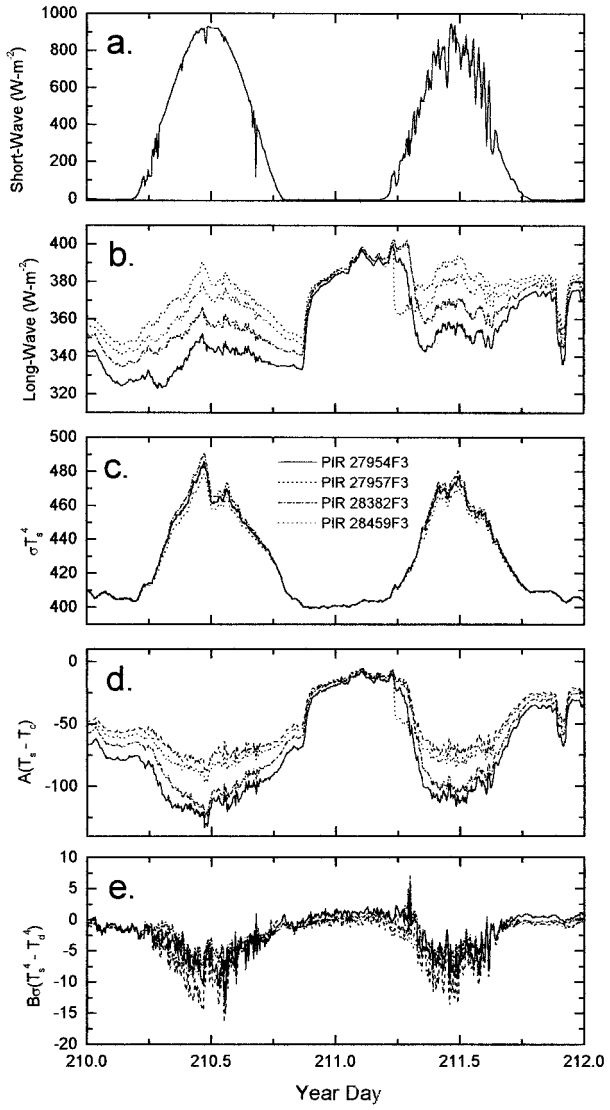

FIG. 11. Details of day 210–211 anomaly: (a) is total shortwave irradiance; (b) is total longwave irradiance from four PIRs; and (c), (d), and (e) are terms 1, 2, and 3 from (1) respectively.

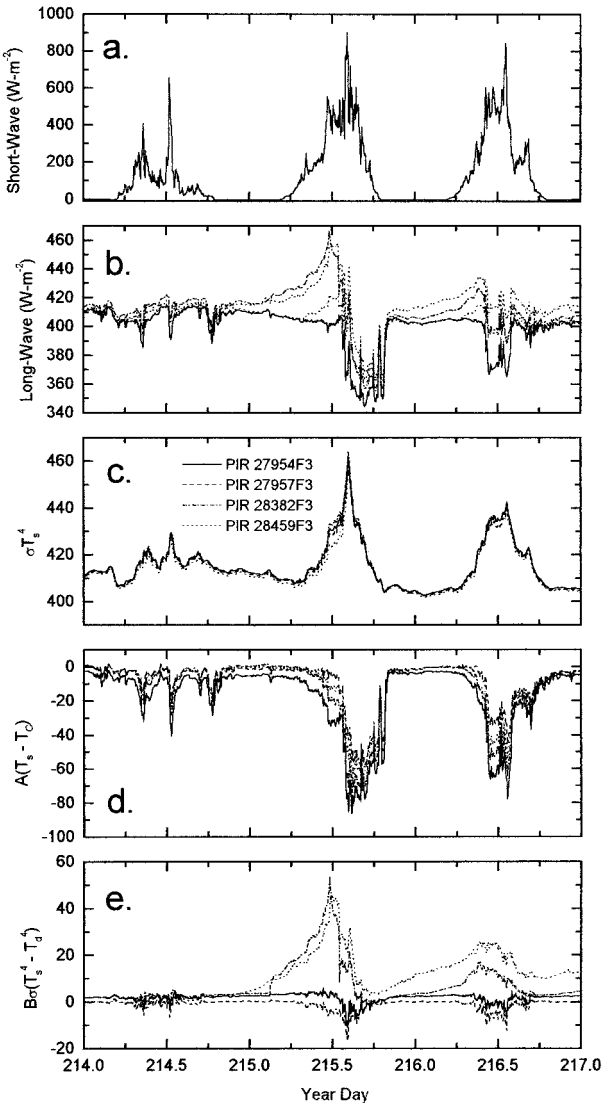

FIG. 12. Details of day 214–216 anomaly: (a) is total shortwave irradiance; (b) is total longwave irradiance from four PIRs; and (c), (d), and (e) are terms 1, 2, and 3 from (1), respectively.

the dome. They could find no problem with the dome in serial number 28460F3 or 27927F3. The signature in the data is clear, an anomalous increase in apparent longwave flux during sunny days proportional to the shortwave irradiance.

Figure 11b illustrates another type of substantial disagreement between PIRs. The four PIRs agree quite well during the night when the thermopile (Fig. 11d) and dome–thermopile (Fig. 11e) radiation exchange terms are close to zero. The daytime shortwave irradiance (Fig. 11a), however, causes the T_s values to differ among the PIRs, and the differences in the thermopile term, although large, fail to compensate. The resulting spread in total longwave flux is up to 40 W m^{-2}. Another disturbing anomaly in the output of one of the PIRs occurs just after dawn on day 211.

A more serious disagreement between sensors is shown in Fig. 12b. The longwave fluxes seen by the PIRs start diverging at the beginning of day 215 with a maximum discrepancy of about 70 W m^{-2}. The discrepancy is due totally to dome temperature (Fig. 12e). Figure 13 shows the meteorological data recorded by a set of IMET modules about 200 m away. Temperatures T_s and T_d follow the air temperature for all four pyrgeometers but at different rates and to differing degrees. A similar situation is seen the next day. Dew forming in different amounts on the four PIRs could explain this anomaly, but it is unlikely that dew could have lasted through even a major part of the 2-day period. The conclusion we draw is that the pyrgeometers do not have identical time constants for their temperature measure-

ments, and rapidly varying conditions can lead to substantial differences in computed longwave flux.

In general, the three-output PIRs in our study, using (1) and our calibration constants, agree in the mean within 10 W m^{-2}. On foggy nights, when terms 2 and 3 in (1) are very close to zero, the PIRs agree predominantly within 5 W m^{-2}. During daylight hours, however, probably due to differing response to fluctuating environmental parameters, the differences in their instantaneous computed total longwave flux can be as much as 50–100 W m^{-2}. We do not know the reason for the higher values.

5. Summary and conclusions

A technique has been described for calibrating the three-output version of the Eppley PIR using equipment available in any well-equipped temperature calibration laboratory and an easily constructed blackbody cavity. It is desirable to calibrate the PIR thermistors since occasional PIRs have thermistors that are up to 0.4°C out of specifications. The results of a number of calibrations on our stock of PIRs are presented.

Fifteen three-output PIRs, calibrated by the techniques described, were run in groups of four in Woods Hole. Thirteen of the 15 had rms deviations of the differences with a common PIR used in all of the groups ranging from 4 to 6 W m^{-2}, in agreement with an estimate of 5.7 W m^{-2} uncertainty in total longwave flux due to uncertainties in the determination of the calibration constants. This is not an evaluation of the absolute accuracy of the PIR, since there is no absolute standard with which to compare it.

The results of the comparison show that individual PIRs can respond differently to rapid changes in atmospheric conditions and that the different responses, particularly in dome temperature, can affect their agreement markedly.

Acknowledgments. Our participation in TOGA COARE was supported by the National Science Foundation, Grant OCE91-10559. Participation in the Pan American Climate Study was supported by the Office of Global Programs, National Oceanic and Atmospheric Administration, Grant NA66GP0130. We thank Dr. R. A. Weller for his pioneering efforts to take longwave observations from buoys and for his useful comments and encouragement. Drs. C. Fairall and F. Bradley participated in useful discussions regarding the results of our findings. We also thank G. Kirk and Eppley Laboratory, Inc. for their cooperation. Helpful comments from the anonymous reviewers are acknowledged. Assistance from all members of the WHOI Upper Ocean Processes Group during all phases of the work as well as assistance from Mary Ann Lucas during the preparation of this manuscript are gratefully acknowledged.

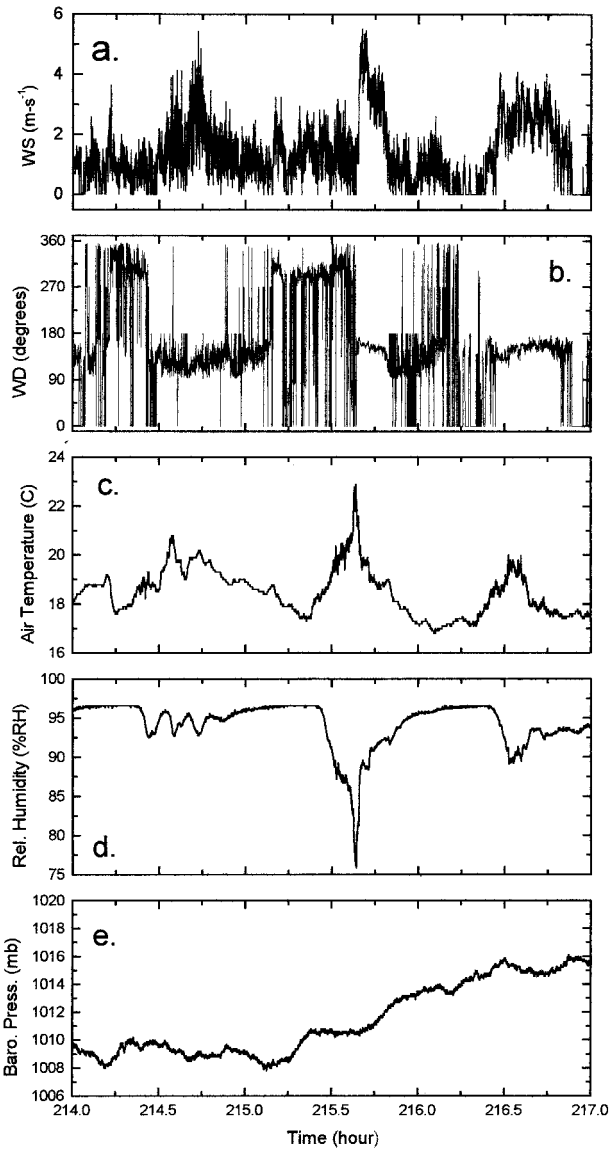

FIG. 13. Meteorological conditions on days 214–216: (a) wind speed, (b) wind direction, (c) air temperature, (d) relative humidity, and (e) barometric pressure.

APPENDIX

PIR Calibration Results

Table A1 is a list of all of the PIR calibrations performed from November 1994 through April 1998 by serial number and calibration date. The techniques were gradually improved from 1994, culminating with the introduction of the Keithley 2000 in April 1996. Also included in the table are the date of the thermistor calibration used (TCAL), the values of *A* and *B* determined, the number of temperature combination runs used (NPTS), and the mean error (MDIFF). This last quantity is the difference between the BBC flux computed from

TABLE A1. PIR calibration.

PIR	Calibration date	TCAL	*A*	*B*	NPTS	MDIFF
27026	19 Apr 96	30 Apr 96	379	2.95	6	−1.3
27026	21 May 96	30 Apr 96	381	3.06	6	−1.0
27026	23 May 96	30 Apr 96	384	3.26	6	0.7
27026	8 Jan 97	6 Jan 97	375	2.79	6	0.6
27026	16 Apr 98	15 Apr 98	380	2.76	6	3.4
27238	4 Apr 96	2 Apr 96	341	3.34	6	1.9
27238	28 May 97	23 May 97	343	3.40	6	−0.3
27363	4 Apr 96	2 Apr 96	355	2.47	6	−0.3
27363	16 Apr 98	15 Apr 98	345	1.87	6	1.6
27927	20 Nov 94	3 Feb 94	394	2.39	5	0.4
27927	23 May 96	3 Feb 94	400	3.70	6	−1.9
27927	28 May 97	23 May 97	405	4.05	6	0.0
27927	1 Dec 97	23 May 97	390	3.58	6	0.0
27928	30 Nov 94	3 Mar 94	389	2.44	4	0.3
27928	2 Mar 95	3 Mar 94	391	2.95	18	0.0
27928	26 Sep 95	3 Mar 94	388	2.26	6	1.1
27928	21 May 96	3 Mar 94	391	2.53	6	−1.0
27928	28 May 97	23 May 97	393	2.75	6	−1.2
27954	20 Nov 94	3 Feb 94	392	2.57	5	−0.5
27954	23 May 96	3 Feb 94	356	3.43	6	−0.4
27954	17 Jul 96	9 Jul 96	362	3.96	6	0.0
27957	26 Jan 95	30 Apr 96	564	5.52	4	0.6
27957	2 Mar 95	30 Apr 96	528	4.91	17	0.3
27957	26 Sep 95	30 Apr 96	532	4.53	6	−1.9
27957	19 Apr 96	30 Apr 96	537	4.52	6	−3.4
27957	17 Jul 96	30 Jul 96	583	5.88	6	−2.3
27957	16 Apr 98	15 Apr 98	529	4.09	6	2.8
28380	4 Apr 96	2 Apr 96	402	3.05	6	5.0
28380	17 Sep 97	15 Sep 97	375	2.43	6	−0.7
28381	4 Apr 96	2 Apr 96	349	2.58	6	−1.3
28381	28 May 97	23 May 97	362	3.50	6	−0.4
28382	19 Apr 96	30 Apr 96	345	2.26	6	−1.6
28382	29 May 97	27 May 97	348	2.55	6	−0.5
28458	26 Jan 95	26 Apr 95	375	2.14	8	−0.1
28458	2 Mar 95	26 Apr 95	366	1.61	19	0.0
28458	26 Apr 95	26 Apr 95	371	2.18	4	−1.0
28458	26 Jul 95	26 Apr 95	354	1.22	4	−0.2
28458	26 Sep 95	26 Apr 95	368	1.82	6	−0.2
28458	21 May 96	26 Apr 95	376	2.15	6	−1.2
28458	17 Sep 97	15 Sep 97	371	0.64	6	−0.2
28459	20 Nov 94	16 Nov 94	420	3.77	4	−0.6
28459	21 May 96	16 Nov 94	423	3.89	6	−2.0
28459	23 May 96	16 Nov 94	417	3.80	6	−2.0
28459	16 Apr 98	15 Apr 98	414	4.14	5	1.6
28460	20 Nov 94	3 Feb 94	414	2.73	5	−0.5
28460	21 May 96	3 Feb 94	412	2.66	6	−1.1
28460	28 May 97	27 May 97	428	4.06	6	−0.9
28461	20 Nov 94	20 May 94	386	2.08	4	−1.8
28461	21 May 96	20 May 94	404	2.69	6	−1.4
28461	23 May 96	20 May 94	390	2.46	6	−1.7
28462	26 Sep 95	5 Apr 94	389	2.54	6	0.4
28462	21 May 96	5 Apr 94	386	2.31	6	−1.0
28462	8 Jan 97	6 Jan 97	345	2.63	6	1.9
28462	1 Dec 97	6 Jan 97	350	2.83	6	−0.4
28463	23 May 96	30 Nov 95	370	2.11	6	−1.8
28463	29 May 97	27 May 97	364	1.90	6	−1.5
28646	26 Jan 95	9 Jan 95	369	2.45	8	−0.7
28872	20 Nov 94	16 Nov 94	376	3.62	5	0.7
28872	26 Sep 95	16 Nov 94	356	1.87	6	2.8
28872	17 Sep 97	15 Sep 97	353	2.00	6	0.5
28908	19 Apr 96	30 Apr 96	339	2.32	6	−0.6
28908	29 May 97	28 May 97	336	2.03	6	−0.7
29379	20 Nov 94	16 Nov 94	358	1.98	5	0.1
29379	26 Sep 95	16 Nov 94	356	1.52	6	0.4
29685	8 Jan 97	6 Jan 97	342	3.32	6	0.6
30924	17 Sep 97	15 Sep 97	386	2.54	6	0.1
31217	17 Jul 96	9 Jul 96	376	3.26	6	2.5

the PIR outputs from the BBC temperature averaged over the runs.

REFERENCES

Albrecht, B., and S. K. Cox, 1977: Procedures for improving pyrgeometer performance. *J. Appl. Meteor.,* **16,** 188–197.

Brogniez, G., J.-C. Buriez, J.-C. van Houtte, and Y. Fouquart, 1986: An improvement of the calibration of the Eppley pyrgeometer for the case of airborne measurements. *Beitr. Phys. Atmos.,* **59,** 538–551.

Drummond, A. J., W. J. Scholes, J. H. Brown, and R. E. Nelson, 1970: A new approach to the measurement of terrestrial longwave radiation. WMO Tech. Note 104.

Eppley Laboratory, Inc., 1976: Instrumentation for the measurement of the components of solar and terrestrial radiation. The Eppley Laboratory, Inc., 12 pp.

——, 1994: Instruction sheet for the Eppley precision infrared radiometer (PIR). The Eppley Laboratory, 5 pp.

Fairall, C. W., P. O. G. Persson, E. F. Bradley, R. E. Payne, and S. A. Anderson, 1998: A new look at calibration and use of Eppley Precision Infrared Radiometers. Part I: Theory and application. *J. Atmos. Oceanic Technol.,* **15,** 1229–1242.

Foot, J. S., 1986: A new pyrgeometer. *J. Atmos. Oceanic Technol.,* **3,** 363–370.

Payne, R. E., A. L. Bradshaw, J. P. Dean, and K. E. Schleicher, 1976: Accuracy of temperature measurements with the VACM. Woods Hole Oceanographic Institution Tech. Rep. WHOI-76-94, 78 pp.

Philipona, R., C. Frohlich, and C. Betz, 1995: Characterization of pyrgeometers and the accuracy of atmospheric long-wave radiation measurements. *Appl. Opt.,* **34,** 1598–1605.

Sparrow, E. M., L. U. Albers, and E. R. G. Eckert, 1962: Thermal radiation characteristics of cylindrical enclosures. *J. Heat Transfer,* 73–81.

Steinhart, T. S., and S. R. Hart, 1968: Calibration curves for thermistors. *Deep-Sea Res.,* **15,** 497–503.

Weller, R. A., and S. P. Anderson, 1996: Surface meteorology and air–sea fluxes in the western equatorial Pacific warm pool during the TOGA Coupled Ocean–Atmosphere Response Experiment. *J. Climate,* **9,** 1959–1990.

——, D. L. Rudnick, R. E. Payne, J. P. Dean, N. J. Pennington, and R. P. Trask, 1990: Measuring near-surface meteorology over the ocean from an array of surface moorings in the Subtropical Convergence Zone. *J. Atmos. Oceanic Technol.,* **7,** 85–103.